Pflügers Arch - Eur J Physiol (2001) 443:115–122
DOI 10.1007/s004240100624

ORIGINAL ARTICLE

A. Whitlock · G. Burnstock · A. J. Gibb

The single-channel properties of purinergic P2X ATP receptors in outside-out patches from rat hypothalamic paraventricular parvocells

Received: 6 March 2001 / Revised: 27 April 2001 / Accepted: 18 May 2001 / Published online: 20 June 2001

Abstract The aim of this study was to characterize functionally the single-channel properties of rat hypothalamic paraventricular medial parvocell purinergic P2X receptors. Single-channel recordings were made from outside-out patches from coronal whole-brain slices from 4-day-old-rats. A heterogeneous population of functional P2X receptors were observed, possibly reflecting a mixture of homomeric $P2X_2$ receptors and heteromers containing $P2X_2$, $P2X_3$, $P2X_4$ or $P2X_6$ subunits. "Flickery" P2X receptor channels with a high open probability (P_o) and chord conductances of 14.4±1.75 and 29.6±0.5 pS at –80 mV were observed in nine patches. The mean open time was 2.51±1.30 ms. In the presence of 1 mM ATP, and excluding long periods of apparent desensitization, these channels had a mean P_o of 0.58±0.29. "Non-flickery" P2X receptors with chord conductances of 16.9± 3.48 and 32.4±3.75 pS, a mean open time of 0.63± 0.15 ms and a mean P_o of 0.01±0.004 at –80 mV were observed in the presence of 1 mM ATP in three patches. P2X receptors showed little apparent concentration dependence in their activity at ATP concentrations of 0.01–1 mM, probably reflecting considerable desensitization. The mean P_o (for all data records) at 10 µM was 0.030±0.017 and 0.030±0.028 at 1 mM.

Keywords Purinoceptor · Hypothalamus · Paraventricular Nucleus · Parvocell

Introduction

The hypothalamic paraventricular nucleus (PVN) is involved in the control of hormone secretion from the anterior and posterior lobes of the pituitary gland, and in the regulation of the autonomic nervous system [32]. The PVN consists predominantly of three classes of cells, all of which express purinergic P2X receptor subunits: the dorsal and medial parvocellular and the posterior magnocellular components [32, 34]. The PVN has been implicated in eliciting eating and satiety [41].

P2X receptors are non-selective, ATP-gated, cation channels permeable to Na^+, K^+ and Ca^{2+} and can mediate rapid (within 10 ms) responses to ATP application. Eight P2X receptor subunits ($P2X_{1–8}$) have been cloned and can combine to form homomeric [3, 4, 5, 7, 9, 12, 16, 28, 33, 39] or heteromeric [17, 19, 20, 21, 30, 37, 38] functional receptors. These may have either a tetrameric [16] or trimeric stoichiometry [28]. Homomeric and heteromeric receptors expressed in *Xenopus* oocytes or in mammalian cells show distinct pharmacological profiles [29].

Despite extensive functional characterisation of homomeric P2X receptors in heterologous expression systems and of native receptors in peripheral neurones, the subunit composition is not known for any native central P2X receptors. Receptor localization techniques, including radioligand binding [1, 2], in situ mRNA hybridization [7, 15, 34, 39], ultrastructural localisation [23] and immunocytochemistry [22, 31, 33, 40, 43, 44], have indicated a widespread distribution of $P2X_{1–4}$ and $P2X_6$ subunits/receptors throughout the adult rat CNS including the hypothalamus in which $P2X_4$ and $P2X_6$ subunits are expressed predominantly. To date, several native functional receptor subunit configurations have been proposed on the basis of electrophysiological, pharmacological and visualisation/localisation studies. Functional rat hippocampal granule cell P2X receptors are thought to be either heteromers of $P2X_4$ and $P2X_6$ subunits or of $P2X_1$, $P2X_2$, $P2X_4$ and $P2X_6$ subunits [42]. Functional heteromeric $P2X_{2+3}$ receptors have been identified in sensory neurons, and the co-expression of $P2X_2$ and $P2X_3$ results in P2X receptors with properties that closely resemble native currents in dorsal root ganglion cells [21].

For the hypothalamus, immunoreactivity, RT-PCR and ultrastructural studies have shown $P2X_2$ receptor expression in the PVN, arcuate nucleus, retrochiasmatic

A. Whitlock · G. Burnstock · A.J. Gibb (✉)
Department of Pharmacology, University College London, Gower Street, London WC1E 6BT, UK
e-mail: uckldag@ucl.ac.uk
Tel.: +44-171-6793747, Fax: +44-171-3807298

area, periventricular nucleus, the ventral part of tuber cinereum area and supraoptic nuclei (SON, in subpopulations of endocrine neurones, neurosecretory and non-neurosecretory axons and dendrites) [15, 40, 43]. RT-PCR and in situ hybridization have demonstrated the expression of mRNAs for $P2X_2$, $P2X_3$, $P2X_4$, $P2X_6$ and $P2X_7$ receptors in the SON and the PVN parvocellular component [34].

This report describes the single-channel properties of native P2X receptors present on PVN medial parvocells. From outside-out patch recordings, at least two distinct populations of receptors are present, ones showing "flickery" openings and ones showing "non-flickery" openings. The distinct populations appear to be comprised of a mixture of homomeric $P2X_2$ receptors and heteromers, perhaps containing $P2X_2$, $P2X_3$, $P2X_4$ and $P2X_6$ subunits.

Materials and methods

Single-channel recordings using brain slices

Single-channel recordings were made at room temperature (21–24 °C) using brain slices obtained from 4-day old Sprague-Dawley rats as previously described [11]. Rats were decapitated and 300-µm-thick, coronal, whole-brain slices were made to include the PVN. Patch pipettes were pulled from borosilicate glass capillaries using a two-stage vertical puller (Narishige PP-83), coated with Sylgard (Dow Corning) and fire-polished (Narishige MF-83) to a final tip diameter of around 1 µm. Pipettes had resistances of 12–16 MΩ when filled with pipette solution. Hypothalamic PVN parvocells were identified visually using a Zeiss Axioskop FS microscope equipped with Nomarski differential interference contrast optics with a total magnification of 640×.

Solutions

The Krebs' solution used for making brain slices had the following composition (mM): sucrose 200, $NaHCO_3$ 25, D-(+) glucose 25, KCl 2.5, NaH_2PO_4 1.25, $CaCl_2$ 1, $MgCl_2$ 2. The Krebs' solution used during patch-clamp recording contained (mM): NaCl 125, $NaHCO_3$ 25, D-(+) glucose 25, KCl 2.5, NaH_2PO_4 1.25, $CaCl_2$ 1 and had a pH of 7.4 following gassing with O_2/CO_2 (95%/5%). All salts and sugars were from BDH. The pipette solution consisted of (mM): CsCl 140, EGTA 10, HEPES 10, $CaCl_2$ 1, adjusted to pH 7.3 using CsOH. ATP was added to the bath in the presence of 10 µM D-(–)-2-amino-5-phosphonovaleric acid (D-AP-5, Sigma) and 40 µM bicuculline methiodide (Sigma) to outside-out patches by manually switching a tap in the inflow to the recording chamber. To prevent degradation of ATP due to spontaneous hydrolysis or the action of ectonucleotidases within the slice, an ATP-regenerating solution was made [24] by including 20 mM phosphocreatine and 10 U/ml creatine phosphokinase in addition to 1 mM ATP (all reagents from Sigma) in the recording Krebs'. The free calcium in the extracellular solution was calculated using the program ALEX by Michel Vivaudou, which is based on [13]. Stability constants for HCO_3^-, HPO_4^-, ATP and phosphocreatine were taken from [36]. The free extracellular $[Ca^{2+}]$ was estimated to be 300 µM when the ATP concentration was 1 mM.

Data analysis

Single-channel currents were amplified using an Axopatch 200A (Axon Instruments, Foster City, Calif., USA), filtered at 10 kHz (–3 dB Bessel) and stored on digital audio tapes (Biologic DTR-1202). Selected records were replayed, filtered at 2 kHz and digitized at 20 kHz using a CED 1401 plus digital interface (Cambridge Electronic Design). Following digitization, single-channel records were analysed by the time-course fitting method using the single-channel analysis program SCAN [8]. Open-time/shut-time distributions are displayed binned logarithmically with a square-root transformation of the ordinate [25, 35]. Dwell-time distributions were fitted using the program EKDIST with a mixture of exponential components using the maximum likelihood method [8]. Distributions of measured channel amplitudes were constructed using openings longer than 2.0 filter rise-times ($2T_r$=332 µs) and fitted with two or three Gaussian components using the maximum likelihood method.

The open probability of the channel (P_o) in the presence of ATP was calculated by dividing the mean open time by the sum of the mean open time and mean shut times. Mean open and shut times were calculated by integration of the exponential components fitted to open- and shut-time distributions respectively.

Results

To obtain maximum receptor activation, initial experiments were performed with an agonist concentration of

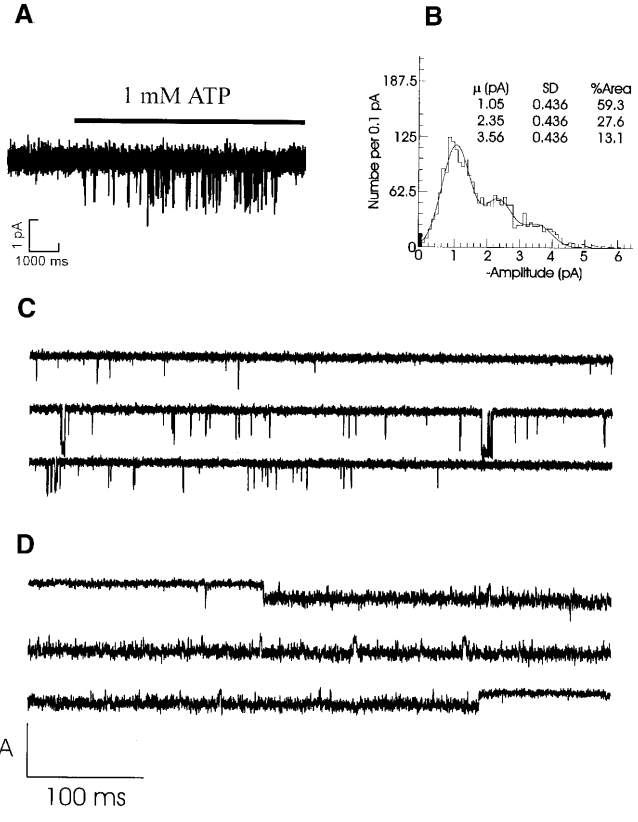

Fig. 1A–D Purinergic P2X receptor activation in response to 1mM ATP. **A** Section of control baseline (–80 mV) followed by ATP application indicated by the *black line*. **B**. Distribution of 7482 channel amplitudes longer than two filter rise-times ($2t_r$=332 µs) from the same outside-out patch. The distribution was best fitted with the sum of three Gaussian components with the standard deviation constrained to be equal between each component. **C**, **D** Contiguous channel traces from the same patch, each illustrating 1.5 s of patch data for "non-flickery" (**C**) and "flickery" (**D**) openings

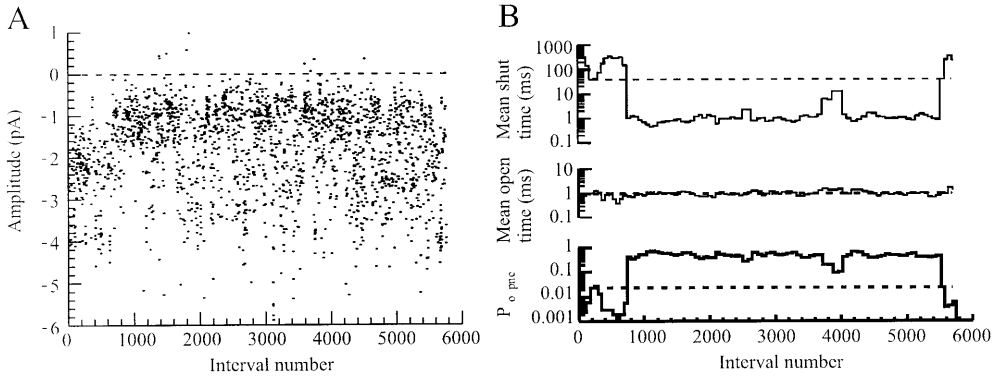

Fig. 2 **A** Amplitude stability plot analysis of all channel openings recorded from an outside-out patch at –80 mV from a 4-day-old rat. The plot shows results from an entire recording made from one patch while exposed to 1 mM ATP. **B** Stability plots illustrating P2X channel mean shut time (*top trace*), mean open time (*middle trace*) and open probability (P_o; *bottom trace*). The data were subsequently separated into high- and low-P_o periods by defining P_o<0.1 as low and P_o>0.1 as high

1 mM ATP. Application of 1 mM ATP evoked channel openings in 18 out of 20 patches. Since each patch was isolated from a different cell, these results suggest that nearly all medial parvocells in the PVN express P2X receptors. A variety of different channel amplitudes were observed, both within individual patches and in different patches, ranging between –0.5 and –3.5 pA at a membrane potential of –80 mV. In addition, P_o varied widely, with periods of high P_o of up to several seconds in duration interspersed with periods of very low P_o. At an agonist concentration of 1 mM, one would expect the receptor to be occupied by the agonist for most of the time (depending on the exact affinity of the agonist for the receptor). These characteristics suggest a heterogeneous population of receptors that enter prolonged periods of desensitisation between periods of high activity.

Figure 1A shows a continuous recording of patch current beginning in control solution (membrane potential: –80 mV) followed by application of 1 mM ATP (black line) that evokes channel openings appearing as downwards deflections from the baseline. In this recording, most channel openings were around –1.0 pA in amplitude, as illustrated in Fig. 1B. The negative of the channel amplitude is plotted so that channel amplitudes appear as positive numbers in the distribution. At –80 mV, the peaks of the Gaussian components correspond to mean current amplitudes (and relative areas) of 3.56 pA (13.1%, observed in only one patch), 2.48±0.13 pA (40.2±12.6%) and 1.28±0.13 pA (68.9±16.0%) corresponding to chord conductances of 45, 31 and 16 pS respectively. Within most recordings, both flickery and non-flickery openings were observed (six out of eight patches). Due to the high P_o of the flickery channels and prolonged periods of activity, components in the amplitude distribution describing non-flickery (low-P_o) channels tend to be obscured. Analysis of channel stability plots was therefore used to identify high- and low-P_o periods in the data record so that the amplitude and kinetic properties of flickery (high-P_o) and non-flickery (low-P_o) channels could be examined separately (Fig. 2B).

Figure 2A illustrates a stability plot for channel amplitudes from a 98-s recording at –80 mV (1 mM ATP). Each point on the plot represents a single-channel amplitude measurement. The most common amplitude level resides around –1 pA with channel openings of between –0.5 and –6 pA (Fig. 2A).

Analysis of non-flickery channels within a patch containing a population of flickery channels was achieved by using the stability plot as a guide to divide the data record into high- and low-P_o sections. Flickery activations resulted in periods of high P_o (approximating to a P_o of 0.8; see Fig. 2B), and the non-flickery channels displayed a P_o of 0.001–0.05 (corresponding to approximately the first 800 intervals in Fig. 2B). This enabled isolation of channel populations based on kinetic properties by analysing separately the high- (>0.1) and low-P_o (<0.1) sections of data.

The amplitude distribution for the high-P_o section of data (Fig. 3A) was best fitted with the sum of two Gaussian components. These had fitted parameters of 2.41 pA (26.3%) and 1.01 pA (73.1%). The main components identified in this way correspond well with the main observed flickery channel amplitudes of 1 pA and 2.5 pA (Fig. 3C). Distributions of channel amplitudes from low-P_o sections of the data (Fig. 3B) were best fitted with the sum of three Gaussian components. Fitted parameters were 3.85 pA (24.2%), 2.17 pA (58.1%) and 1.22 pA (17.7%). Figure 3D displays examples of channel openings corresponding to the main components observed in the low-P_o amplitude distributions. These distributions suggest that PVN cells express a heterogeneous population of P2X receptors.

For high-P_o data (mean P_o 0.58±0.29) the mean (flickery) channel amplitudes (and relative areas) at –80 mV were 2.37±0.04 pA (20.3±6.05%) and 1.16±0.15 pA (79.5±6.35%), corresponding to chord conductances of 30 and 14 pS respectively. Low-P_o (mean P_o 0.01±0.004), non-flickery channel amplitudes (and relative areas) were 3.85 pA (8.1%, observed in only one patch), 2.16±0.25 pA (47.2±8.4%) and 1.17±0.20 pA (44.8±15%), corresponding to chord conductances of 48, 27 and 15 pS respectively.

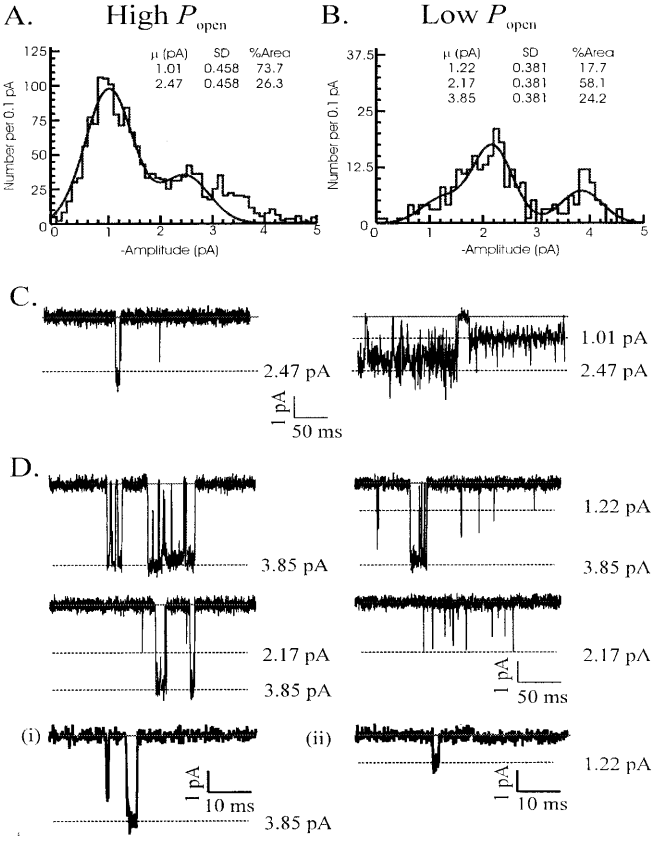

Fig. 3A–D Amplitude of channel openings in either high- or low-P_o sections. **A** Distribution of channel amplitudes longer than two filter rise-times during high-P_o periods. Membrane potential –80 mV. The distribution is fitted with the sum of two Gaussian components with the standard deviation constrained to be the same for both components. The component corresponding to openings ~3.5 pA was not fitted as it represents double openings of 2.46- and 0.99-pA channels. **B** Distribution of the amplitude of channel openings longer than two filter rise-times observed during low-P_o periods. **C** Channel traces illustrating high-P_o openings identified from the stability plot analysis shown in **A** and **B**. **D** Channel traces illustrating low-P_o openings identified from the stability plot analysis shown in **A** and **B**; *i*, *ii*: channel traces illustrating low-P_o openings on a faster time scale than those *above*

Current/voltage (*I*/*V*) relationships were constructed for channel amplitudes measured in the low- and high-P_o sections for each patch. However, given that there are multiple conductance levels in each patch, and that previous reports have shown that some native P2X receptors as well as homomeric $P2X_2$ receptors have inwardly rectifying single-channel conductances, the heterogeneous P2X receptor population observed here may include receptors with both linear and inwardly rectifying single-channel currents. This makes assignment of amplitude levels measured at each voltage to individual *I*/*V* relations problematic. Currently, the flickery and non-flickery channels, have been segregated only on the basis of their P_o. However, the data obtained does not indicate whether the distinct amplitudes obtained for either flickery or non-flickery channels, arise from the same receptor, perhaps alternating between different gating modes, or from different receptors. Figure 4 displays examples of channel openings observed at different membrane potentials during a single recording. These data illustrate the fact that similar channel types were observed at each membrane potential between –80 mV and –20 mV, given the proviso that the resolution of the recording is less at –20 mV because of the smaller driving force for current through the channel. The right hand panel of the figure shows examples of high-P_o flickery channel activity seen at each membrane potential. The examples shown illustrate the main classes of channel amplitude identified from the Gaussian components fitted to the amplitude distributions. Figure 5A shows the single-channel *I*/*V* relationships for the different conductance levels identified by fitting the amplitude distributions. No linear regression of the data was attempted, given the possible existence of inwardly rectifying and linear *I*/*V* relationships within each data set.

Separation of the high- and low-P_o sections allowed distinction between the *I*/*V* relationships for the flickery (Fig. 5B) and non-flickery openings (Fig. 5C). No flickery openings were observed at positive potentials (+20 mV, +40 mV and +60 mV, n=3 patches), although the small data sample here means that this could also be due to prolonged desensitization at positive potentials. Recordings at each positive and negative potential were of the same duration (120 s). However, in the presence of ATP, clear non-flickery channel openings were evident at positive voltages. Interestingly, between –40 and –80 mV, the *I*/*V* relationship for the high-P_o flickery channel tended towards outwards rectification.

Low-P_o openings had an approximately linear *I*/*V* relationship at negative membrane potentials and non-flickery openings were also observed at positive potentials. Only at –70 mV and –80 mV was a third component evident in the amplitude distribution. The data for the two most evident amplitude components were fitted by linear regression constrained to pass through the origin, giving slope conductances of 51 and 29 pS. These correspond well with the chord conductances measured at –80 mV of 48, 27 and 15 pS. Other non-flickery channel amplitudes were also observed, but occurred too rarely to be characterised accurately.

Figure 6 shows the open-time distributions for the patch illustrated in Fig. 1. Distributions of channel open periods were best fitted with the sum of two or sometimes three exponential components. Recordings at –80 mV had mean time constants (τ) (and relative areas) of τ_1=0.09±0.04 ms (37.2±16.2%), τ_2=1.10±0.55 ms (40.1±8.00%) and τ_3=4.46±1.42 ms (22.7±11.3%). The distribution means averaged 1.67±0.86 ms at –80 mV. Figure 6A shows all the data for the one patch. These were best fitted with two exponential components. The mean open time was 0.83 ms and the fit predicts that there were 5344 apparent openings in the data record.

Shut-time distributions were usually best fitted with the sum of five (sometimes four) exponential components for all patch data. At –80 mV, mean shut-time distribution time constants (and relative areas) were

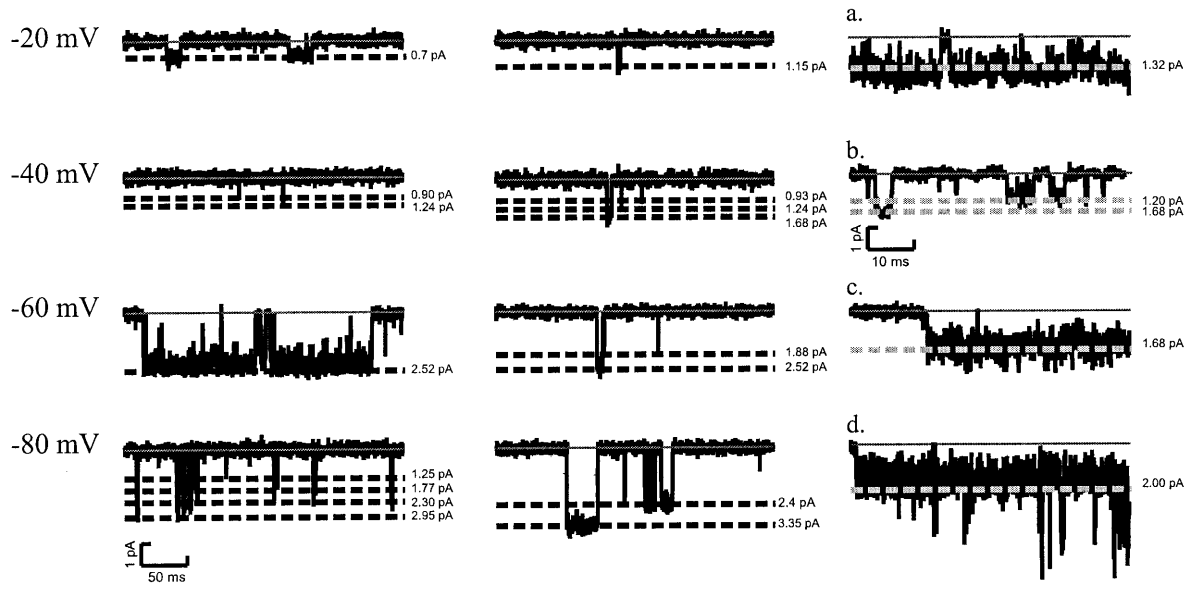

Fig. 4 Voltage dependence of P2X channel currents observed in the presence of 1 mM ATP at membrane potentials of –20, –40, –60 and –80 mV. All examples from the same patch. Inwards currents are shown as *downwards deflections* from the *baseline*. Examples illustrate the main classes of channel amplitude identified from the Gaussian components fitted to the amplitude distributions. *Dashed lines* are drawn at the mean of the relevant Gaussian component fitted to the amplitude distribution. The data were low-pass filtered at 2 kHz and digitized at 20 kHz. High-P_o flickery channels are labelled *a*, *b*, *c*, and *d*

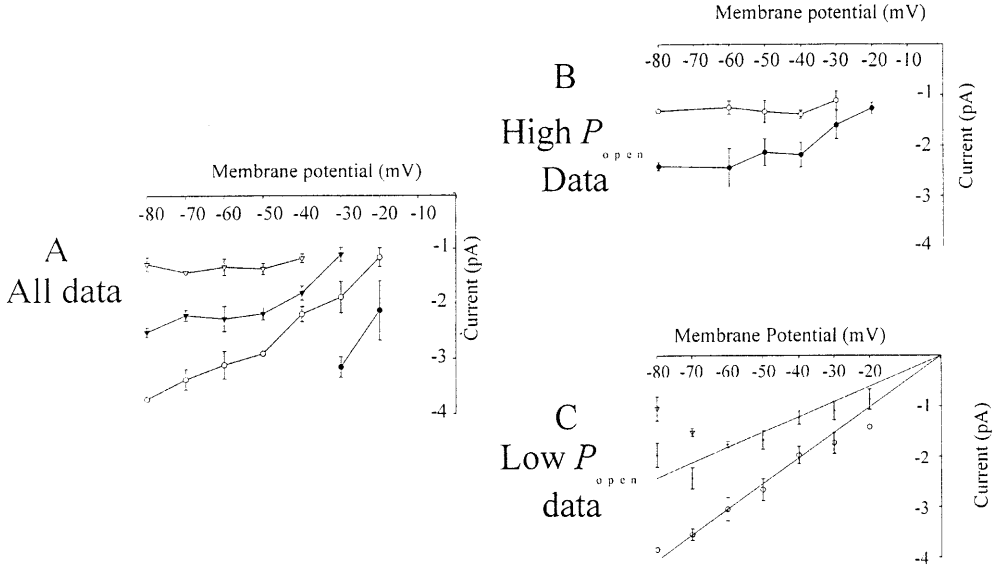

Fig. 5A–C Relationships between single-channel current amplitude and patch potential (n=6 patches). Means±SEM of the mean-single channel current obtained from Gaussian fits to the fitted amplitude distributions obtained at each membrane potential for the all the data. **A** Current/voltage (*I*/*V*) relationship for all data. **B** *I*/*V* relationship for high-P_o sections. **C** *I*/*V* relationship for channel amplitudes found in low.P_o sections. A linear *I*/*V* relationship was assumed, as non-flickery openings were also observed at positive membrane potentials

τ_1=0.12±0.07 ms (27.0±10.5%); τ_2=0.71±0.33 ms (45.3±18.6%); τ_3=14.0±5.60 ms (5.40±1.24%), τ_4=155±49.9 ms (19.2±14.0%) and τ_5=1132±422 ms (3.07±0.55%). The distribution means averaged 63.2±31.8 ms at –80 mV.

Separation of high- and low-P_o periods within each patch allowed examination of the distribution of open and closed times within these components of the data. Figure 6C and D illustrates the open-time distributions obtained from high- and low-P_o periods. Open-time distributions from segregated high- or low-P_o periods were qualitatively similar to distributions of all open times in the recording. For the high-P_o periods in the patch shown in Figure 6C the mean channel open time was 0.74 ms; the low P_{open} periods (Figure 6D) had a mean open time of 1.19 ms. At –80 mV the mean open time within high-P_o periods was 2.51±2.06 ms, that for low-P_o periods was 0.63±0.19 ms. Thus although there was a tendency for longer open times within high-P_o periods further experiments are required to determine if this is significant. The effect of changing the membrane potential on the mean open time is shown in Fig. 6B. Linear regression of the data shown in Fig. 6B did not give a slope significantly different from zero. Although there is a clear trend for longer open times at less negative potentials, this may be partly due to the lower resolution

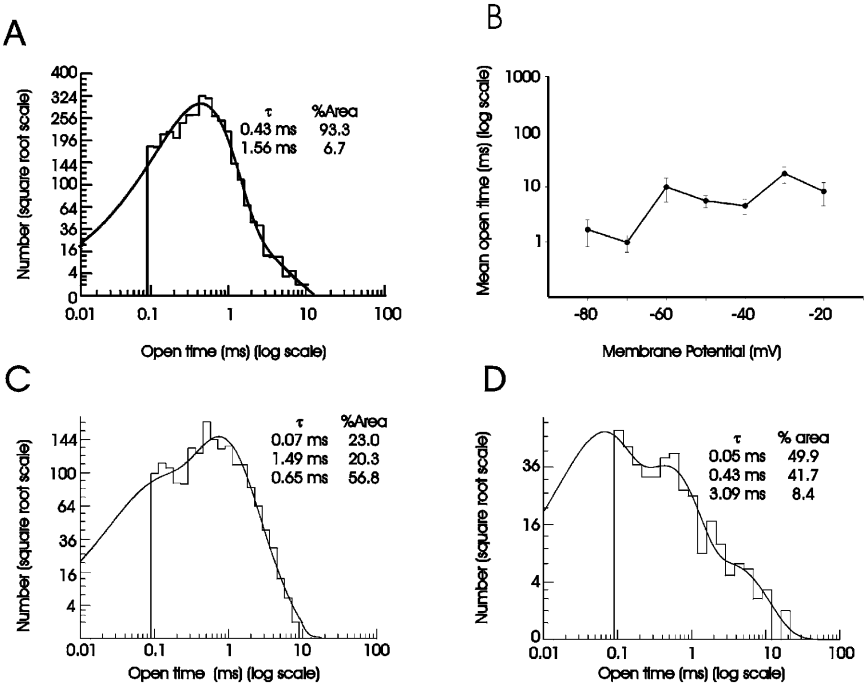

Fig. 6A–D Open-time distributions and voltage dependence of channel open times in the presence of 1 mM ATP. **A**, **C** and **D** Open-time distributions from the patch shown in Fig. 1. The square root of bin frequency (*abscissa*) is shown as a function of the time (log scale, *ordinate*) [25, 35]. This transformation converts the normal exponential distribution into a peaked one, with the peaks corresponding to the time constants of the exponential components. **A** Distribution of 3756 open periods of 0.09–20 ms duration. **B** Relationship between membrane potential and mean open time for the data in **A**. The data in **A** were subsequently separated into high- (**C**) and low- (**D**) P_o distributions

at less negative voltages that results in many short closings being missed.

The concentration dependence of P2X receptor activation was investigated by application of 10 µM, 100 µM and 1 mM ATP to outside-out patches (n=3) held at –60 mV for 3 min at each concentration (control solution washed on between concentrations). The most common channel amplitude at all three concentrations was around 1 pA: 0.97±0.1 pA (92±7.8%), 0.94±0.18 pA (86±15%), 1.03±0.06 pA (60±16%) for 10 µM, 100 µM and 1 mM ATP respectively. In addition, channel openings averaging 1.86±0.06 pA (25±14%) and 2.68±0.03 pA (14±4%) were observed consistently at 1 mM ATP but were only rarely at the lower ATP concentrations. Increasing the ATP concentration from 10 µM to 1 mM decreased the mean shut time slightly. The mean open time similarly showed little concentration dependence. These values may reflect the presence of desensitization within the low-P_o data sets or increased high-P_o channel activity within patches with increased ATP concentration masking changes in the low-P_o channel activity.

Discussion

The results presented here provide the first description of the single-channel properties of native P2X receptors from rat PVN medial parvocells. The characteristics of PVN P2X receptors are consistent with a physiological role in mediating fast synaptic transmission [10]. Two distinct populations of P2X receptor in medial parvocells have been identified, referred to here as the flickery and non-flickery receptors. Both species of P2X receptor have unique single-channel characteristics compared with other native and recombinant P2X receptors.

The relatively high density of P2X receptor subunit mRNA [7, 15] and protein [23, 34, 43] in the PVN is reflected by functional P2X receptors being present in 18 out of 20 patches examined in this study (of which 8 were analysed in detail).

Within flickery and non-flickery populations, multiple conductance states differing between patches suggest there are multiple low- and high-P_o channel types. However, whether they are due to one channel opening to several conductance levels, or modal changes in gating kinetics giving rise to flickery and non-flickery activation states, still has to be determined.

The high-P_o flickery channels (observed in a total of 18 patches of which 6 were analysed in detail) are similar in their flickery nature to the homomeric $P2X_2$ receptors [9] and homomeric $P2X_1$, $P2X_2$ and $P2X_4$ receptors [12]. The flickery, high-P_o channels had chord conductances of 30 and 14 pS (n=3 patches; 1 mM ATP) at –80 mV.

Flickery channels were not observed at positive potentials and so may be inwardly rectifying. However, they were also not observed at –70 mV and –30 mV (possibly because of coincident receptor desensitization) and so may simply have not been observed at positive potentials because the receptors happened to be desensitized when the membrane potential was stepped to positive voltages.

Homomeric $P2X_1$, $P2X_2$ and $P2X_4$ receptors expressed in CHO cells [12], exhibit chord conductance values of 18 ($P2X_1$), 21 ($P2X_2$) and 9 pS ($P2X_4$) at –100 mV (in 0.3 mM extracellular calcium). Homomeric $P2X_3$ receptor channels are reportedly too flickery to determine the single-channel conductance accurately [12]. The chord conductance values of homomeric $P2X_1$ and

$P2X_2$ receptors are similar to those of the flickery channels observed in this study of 16 pS.

Homomeric $P2X_2$ receptors expressed in HEK cells and oocytes produce a flickery single channel conductance of 16 pS [9]. Native flickery channels have been observed in rat hippocampal granule cells (chord conductance 31 pS in 0.3 mM calcium; –60 mV) [42], and sensory ganglia (chord conductance 35 pS in 0.1 mM extracellular calcium; –75 mV) [18]. The observed flickery 29.6-pS channel (–80 mV) observed in this study exhibited similar single-channel properties, possibly implying a subunit composition similar to that in ganglia and hippocampal granule cells.

The flickery gating observed is different to that observed by Wong et al. [42], in that despite the same filter and digitisation settings, it exhibited fused rapid transitions between a full open and shut state within an opening. However, the flickery channels observed here exhibited a greater gating homology to homomeric $P2X_2$ receptors expressed in HEK cells and oocytes [9], whereby rapid transitions between full open and shut states within the complete opening were not resolved. These differences could be due to varying subunit composition of the native channel(s).

Non-flickery openings had mean chord conductances of 48, 27 and 15 pS. Rat superior cervical ganglia exhibit a similar chord conductance to the observed 15-pS channels (12 pS; –80 mV) [6]. Similarly, PC12 cells exhibit a chord conductance of 13 pS (–150 mV) [26, 27]. Other PC12 chord conductances (11, 23 and 29 pS, [26]) are also similar to the chord conductances observed in this study. Given that the rat $P2X_2$ receptor subunit was originally cloned from a PC12 cell cDNA library [4] these data support the hypothesis that the $P2X_2$ subunit is present in medial parvocell P2X receptors.

Interestingly, large-conductance, 63-pS P2X channels recorded in cardiac ganglia [14] and a 55-pS, large-conductance channel from hippocampal granule cells [42] have been reported. Medial parvocells also exhibit large-conductance, non-flickery channels (48 pS). In the hippocampus, the 55-pS channel was suggested to be formed from either co-assembly of heteromeric $P2X_{4+6}$, or of $P2X_1$, $P2X_2$, $P2X_4$ and $P2X_6$ [42].

Open-time distributions for the high- and low-P_o P2X receptors were best fitted with two or three exponential components, implying that the receptors exist in a minimum of two, distinct, open states. However, given the evident heterogeneous nature of P2X channels within each patch, and the multiple conductance levels of flickery and non-flickery openings observed, it is impossible to distinguish between individual receptors opening to more than one discrete open state or the presence of multiple receptor types in the patch. Further experiments will be needed to clarify the open-state properties of medial parvocellular P2X receptors.

Open-time distributions for homomeric recombinant $P2X_2$ receptors were best fitted with two exponential components, with time constants of approximately 0.3 and 2 ms (10 μM ATP; –120 mV) [9]. In the present report, high-P_o flickery openings activated by 10 μM ATP produced mean open time constants of 0.63, 3.23 and 22.7 ms (–60 mV; n=3). The initial two (fastest) components are similar to the values for homomeric $P2X_2$ receptors. However, given the heterogeneous nature of the flickery channel activations found in PVN medial parvocells, these values may not apply to just one channel population. Pharmacological tools are needed to isolate the different channel types further in medial parvocells.

The electrophysiological evidence presented here suggests that the high-P_o flickery openings have similar single-channel conductances to those of sensory ganglia [18], flickery channels in hippocampal granule cells [42] and PC12 cells [26, 27]. The hippocampal flickery channels may consist of similar subunits to those of dorsal root ganglia, shown to express functionally $P2X_2$ and $P2X_3$ receptor subunits capable of forming functional heteromeric $P2X_{2+3}$ receptors [21]. However, since the single-channel conductance of recombinant $P2X_{2+3}$ receptors has not yet been reported, it is not clear whether the flickery channel could be composed of $P2X_2$ and $P2X_3$ subunits. Given the high $P2X_2$ subunit expression within the PVN [7, 23, 34, 40, 43] it seems likely that the $P2X_2$ subunit is expressed functionally here either as a homomeric receptor or as part of a heteromeric complex. High levels of $P2X_3$ receptor subunit expression have been identified within the PVN [7, 34]. Whether they form functional heteromeric $P2X_{2+3}$ receptors similar to those in dorsal root ganglia, or homomeric $P2X_3$ receptors, could be investigated using pharmacological tools.

The non-flickery openings, similar to the large-conductance channel observed in cardiac ganglia [14] and hippocampal granule cells [42], could have a similar subunit composition to receptors in the hippocampus. $P2X_4$ and $P2X_6$ subunits are expressed within the PVN [7, 34] and may form either heteromers of $P2X_4$ and $P2X_6$ subunits or form heteromers which also contain $P2X_1$ and/or $P2X_2$ subunits, as suggested for hippocampal receptors [42].

In conclusion, this study supports current hypothalamic purinergic research indicating a heterogeneous functional P2X receptor population within the rat hypothalamus. Further experiments involving the single-channel properties and pharmacology of P2X receptors in PNV medial parvocells are needed to define more clearly the subunit composition of these native P2X receptors. In addition, this characterization of P2X receptor properties in this nucleus forms a valuable background to any future experiments investigating possible fast synaptic transmission in the PVN mediated by P2X receptors.

References

1. Balcar V, Li Y, Killinger S, Bennett MR (1995) Autoradiography of P2X ATP receptors in the rat brain. Br J Pharmacol 115:302–306
2. Bo X, Burnstock G (1994) Distribution of ^{3}[H]-methylene ATP binding sites in rat brain and spinal cord. Neuroreport 5:1601–1604

3. Bo X, Schoepfer R, Burnstock G (2000) Molecular cloning and characterization of a novel ATP P2X receptor subtype from embryonic chick skeletal muscle. J Biol Chem 12: 14401–14407
4. Brake AJ, Wagenbach MJ, Julius D (1994) New structural motif for ligand-gated ion channels defined by an ionotropic ATP receptor. Nature 371:519–523
5. Chen CC, Akopian AN, Sivilotti L, Colquhoun D, Burnstock G, Wood JN. (1195) A P2X purinoceptor expressed by a subset of sensory neurons. Nature 377:428–431
6. Cloues R (1995) Properties of ATP-gated channels recorded from rat sympathetic neurons: voltage dependence and regulation by Zn^{2+} ions. J Neurophysiol 73:312–319
7. Collo G, North RA, Kawashima E, Merlo-Pich E, Neidhart S, Surprenant A, Buell G (1996) Cloning of $P2X_5$ and $P2X_6$ receptors, and the distribution and properties of an extended family of ATP-gated ion channels. J Neurosci 16: 2495–2507
8. Colquhoun D, Sigworth FJ (1995) Fitting and statistical analysis of single channel records. In: Sakmann B, Neher E (eds) Single channel recording, 2nd edn. Plenum Press, New York, pp 483–588
9. Ding S, Sachs F (1999) Single channel properties of $P2X_2$ purinoceptors. J Gen Physiol 11:695–720
10. Edmonds B, Gibb AJ, Colquhoun D (1995) Mechanisms of activation of glutamate receptors and the time course of excitatory synaptic currents. Annu Rev Physiol 57:495–519
11. Edwards FA, Konnerth A, Sakmann B, Takahashi T (1989) A thin slice preparation for patch clamp recordings from neurones of the mammalian central nervous system. Pflügers Arch 414:600–612
12. Evans RJ (1996) Single channel properties of ATP-gated cation channels (P2X receptors) heterologously expressed in Chinese hamster ovary cells. Neurosci Lett 212:212–214
13. Fabiato A (1988) Computer programs for calculating total from specified free or free from specified total ionic concentration in aqueous solutions containing multiple metals and ligands. Methods Enzymol 157:378–417
14. Fieber LA, Adams DJ (1991) Adenosine triphosphate-evoked currents in cultured neurones dissociated from rat parasympathetic cardiac ganglia. J Physiol (Lond) 434:239–256
15. Kidd EJ, Grahames CBA, Simon J, Michel AD, Barnard EA, Humphrey PPA (1995) Localization of P2X purinoceptor transcripts in the rat nervous system. Mol Pharmacol 48:569–573
16. Kim M, Yoo OJ, Choe S (1997) Molecular assembly of the extracellular domain of $P2X_2$, an ATP-gated ion channel. Biochem Biophys Res Commun 240:618–622
17. King BF, Townsend-Nicholson A, Wildman SS, Thomas T, Spyer KM, Burnstock G. (2000) Coexpression of rat $P2X_2$ and $P2X_6$ subunits in *Xenopus* oocytes. J Neurosci 20:4871–4877
18. Krishtal OA, Marchenko SM, Obukhov AG (1988) Cationic channels activated by extracellular ATP in rat sensory neurons. Neuroscience 27:995–1000
19. Lê KT, Babinski K, Séguéla P (1998) Central $P2X_4$ and $P2X_6$ channel subunits coassemble into a novel heteromeric ATP receptor. J Neurosci 18:7152–7159
20. Le KT, Boue-Grabot E, Archambault V, Séguéla P (1999) Functional and biochemical evidence for heteromeric ATP-gated channels composed of $P2X_1$ and $P2X_5$ subunits. J Biol Chem 274:15415–15419
21. Lewis C, Neidhart S, Holy C, North RA, Buell G, Surprenant A (1995) Coexpression of $P2X_2$ and $P2X_3$ receptor subunits can account for ATP-gated currents in sensory neurons. Nature 377:432–435
22. Loesch A, Burnstock G (1998) Electron-immunocytochemical localization of P2X1 receptors in the rat cerebellum. Cell Tissue Res 294:253–260
23. Loesch A, Miah S, Burnstock G (1999) Ultrastructural localisation of ATP-gated $P2X_2$ receptor immunoreactivity in the rat hypothalamo-neurohypophysial system. J Neurocytol 28:495–504
24. MacDonald JF, Mody I, Salter MW (1989) Regulation of *N*-methyl-D-aspartate receptors revealed by intracellular dialysis of murine neurones in culture. J Physiol (Lond) 414:17–34
25. McManus OB, Blatz AL, Magleby KL (1987) Sampling, log binning, fitting and plotting durations of open and shut intervals from single channel and the effects of noise. Pflügers Arch 418:530–533
26. Nakazawa K, Hess P (1993) Block by calcium of ATP-activated channels in pheochromocytoma cells. J Gen Physiol 101: 377–392
27. Nakazawa K, Inoue K, Fujimori K, Takanaka A (1990) ATP-activated single-channel currents recorded from cell-free patches of pheochromocytoma PC12 cells. Neurosci Lett 119:5–8
28. Nicke A, Baumert HG, Rettinger J, Eichele A, Lambrecht G, Mutschler E, Schmalzing G (1998) $P2X_1$ and $P2X_3$ receptors form stable trimers: a novel structural motif of ligand-gated ion channels. EMBO J 17:3016–3028
29. North RA, Surprenant A (2000) Pharmacology of cloned P2X receptors. Annu Rev Pharmacol Toxicol 40:563–580
30. Radford KM, Virginio C, Surprenant A, North RA, Kawashima E (1997) Baculovirus expression provides direct evidence for heteromeric assembly of $P2X_2$ and $P2X_3$ receptors. J Neurosci 17:6529–6533
31. Rubio ME, Soto F (2001) Distinct localization of P2X receptors at excitatory postsynaptic specializations. J Neurosci 21:641–653
32. Sawchenko PE, Brown ER, Chan RK, Ericsson A, Li HY, Roland BL, Kovacs KJ (1996) The paraventricular nucleus of the hypothalamus and the functional neuroanatomy of visceromotor responses to stress. Prog Brain Res 107:201–222
33. Seguela P, Haghighi A, Soghomonian JJ, Cooper E (1996) A novel neuronal P2X ATP receptor ion channel with widespread distribution in the brain. J Neurosci 16:448–455
34. Shibuya I, Tanaka K, Hattori Y, Uezono Y, Harayama N, Noguchi J, Ueta Y, Izumi F, Yamashita H (1999) Evidence that multiple P2X purinoceptors are functionally expressed in rat supraoptic neurones. J Physiol (Lond) 514:351–367
35. Sigworth FJ, Sine SM (1987) Data transformations for improved display and fitting of single-channel dwell time histograms. Biophys J 52:1047–1054
36. Smith RM, Martell AE (1982) Critical stability constants. Plenum Press, New York
37. Surprenant A, Schneider DA, Wilson HL, Galligan JJ, North RA (2000) Functional properties of heteromeric $P2X_{(1/5)}$ receptors expressed in HEK cells and excitatory junction potentials in guinea-pig submucosal arterioles. J Auton Nerv Syst 81:249–263
38. Torres GE, Haines WR, Egan TM, Voigt MM (1998) Coexpression of $P2X_1$ and $P2X_5$ receptor subunits reveals a novel ATP-gated ion channel. Mol Pharmacol 54:989–993
39. Valera S, Hussy N, Evans RJ, Adami N, North RA, Surprenant A, Buell G (1994) A new class of ligand-gated ion channel defined by P2X receptor for extracellular ATP. Nature 371:516–519
40. Vulchanova L, Arvidsson U, Riedl M, Wang J, Buell G, Surprenant A, North RA, Elde R (1996) Differential distribution of two ATP-gated ion channels (P_{2X} receptors) determined by immunocytochemistry. Proc Natl Acad Sci USA 93:8063–8067
41. Wellman PJ (2000) Norepinephrine and the control of food intake. Nutrition 16:837–842
42. Wong AYC, Burnstock G, Gibb AJ (2000) Single channel properties of P2X ATP receptors in outside-out patches from rat hippocampal granule cells. J Physiol (Lond) 527: 529–547
43. Xiang Z, Bo X, Oglesby I, Ford A, Burnstock G (1998) Localization of ATP-gated $P2X_2$ receptor immunoreactivity in the rat hypothalamus. Brain Res 813:390–397
44. Yao ST, Barden JA, Finkelstein DI, Bennett MR, Lawrence AJ (2000) Comparative study on the distribution patterns of P2X(1)-P2X(6) receptor immunoreactivity in the brainstem of the rat and the common marmoset (*Callithrix jacchus*): association with catecholamine cell groups. J Comp Neurol 427: 485–507